Effect of coated mesh wick on the performance of cylindrical heat pipe using graphite nanofluids

P. R. Jyothi Sankar[1] · S. Venkatachalapathy[1] · Lazarus Godson Asirvatham[2] · Somchai Wongwises[3]

Abstract

Thermal performance evaluation of TiO_2-coated copper mesh wick in a cylindrical heat pipe with graphite nanofluid is experimentally analyzed at various inclinations, nanoparticle concentrations and power levels. Boiling heat transfer from the evaporator of a heat pipe depends on both thermal conductivity of the nanoparticle and suspension stability of the nanofluid. The lower the density of the nanoparticle, the better the suspension stability. Spherical graphite nanoparticles having lower density and good thermal conductivity quicken the heat transfer rate and hence the vaporization of base fluid. A hydrophilic coating of TiO_2 is done on the copper wick structure to reduce the contact angle of graphite nanofluid. Results showed that the heat pipe worked well at 60° inclination compared to the other tested orientations. For this optimum condition, a reduction in 168.75% of thermal resistance is obtained compared with DI water with uncoated wick at horizontal position and also an improvement in thermal efficiency of 94.07% for 1.0 mass% particle loading. The enhancement in equivalent thermal conductivity is 90.87% for 1.0 mass% compared with DI water. Results from the repeatability test also confirm that the hydrophilic coating over the wick is stable, and results are repeatable.

List of symbols

A	Area (m^2)
C_p	Specific heat ($J\,kg^{-1}\,K^{-1}$)
d	Outer diameter (mm)
I	Current (A)
k	Thermal conductivity ($W\,m^{-1}\,K^{-1}$)
L	Length (mm)
$\dot{m}$	Mass flow rate ($kg\,s^{-1}$)
Q	Input power (Heat supplied) (W)
q	Heat flux ($W\,m^{-2}$)
R	Thermal resistance ($K\,W^{-1}$)
T	Temperature (K)
ΔT	Temperature difference (K)
V	Voltage (V)
Mass.	Mass fraction (%)

Abbreviations

CW	Coated wick
UCW	Uncoated wick

Subscripts

av	Average
bf	Base fluid
c	Condenser
cs	Cross-section
cv	Condenser vapor
cw	Condenser wall
ec	Evaporator−condenser
Eq.	Equivalent
ev	Evaporator vapor
ew	Evaporator wall
np	Nanoparticle
o	Overall
w	Water
th	Thermal

✉ P. R. Jyothi Sankar
jyothisankar74@gmail.com

1 Department of Mechanical Engineering, National Institute of Technology Tiruchirappalli, Tiruchirappalli 620015, Tamil Nadu, India

2 Department of Mechanical Engineering, Karunya Institute of Technology and Sciences, Coimbatore, Tamil Nadu 641114, India

3 Fluid Mechanics, Thermal Engineering and Multiphase Flow Research Lab (FUTURE), Department of Mechanical Engineering, Faculty of Engineering, King Mongkut's University of Technology Thonburi, Bangmod, Bangkok 10140, Thailand

Greek symbols

Δ Increment
η Efficiency (%)

Introduction

Heat pipes are efficient two-phase heat transfer devices employing a working fluid to transfer the heat. The heat pipe was first developed by Gaugler in the year 1942 [1]. Since its invention, the quest for enhancing the performance is growing day by day and also their applications in multidisciplinary fields [2, 3] such as cooling of electronic chips in computers and electronic industries, fuel cells, solar collectors, nuclear power, desalination systems, space and defense applications. Cheng et al. [4] stated that the physical properties of nanofluids have a significant effect on the boiling heat transfer characteristics. The performance of a heat pipe can be enhanced by improving the thermophysical properties of working fluid. An easiest and effective way to enhance the heat transfer properties of the working fluid is by the addition of highly conducting solid nanoparticles into the base fluid.

Even though James Clerk Maxwell proposed the idea of dispersing solid particles into liquids well before, the usage of nanoparticle dispersion in liquids came into practice during the year 1996 and it was originated from a research group at the Argonne National Laboratory, USA, in an attempt to increase the thermal conductivity of base fluid. Thermally conducting metallic and nonmetallic particles of 1–100 nm size are dispersed into the base fluid and are called nanofluids. Since then, several studies were carried out with a focus on the measurement techniques and evaluation of thermal conductivity of nanofluids. In an attempt to make a unified approach for thermal conductivity measurement techniques and their values, bench mark studies were carried out by leading organizations around the world and the results were summarized and reported by Buongiorno et al. [5] on INPBE (International Nanofluid Property Benchmark Exercise).

Recent studies on heat pipes established the fact that the addition of nanoparticles in the working fluid would impart a significant improvement on the thermal performance and hence the efficiency [6–22]. Experimental studies were conducted by Putra et al. [6] to estimate the thermal resistance of mesh wick cylindrical heat pipes with different nanofluids, viz. Al_2O_3/DI water, Al_2O_3/ethylene glycol (EG), TiO_2/DI water, TiO_2/EG and ZnO/EG. The volume fraction of the nanofluids was varied from 1 to 5%, and the maximum input power was 30 W. A lowest thermal resistance of 0.26 °C W^{-1} was obtained for Al_2O_3/DI water with 5% volume concentration at the maximum power, whereas it was 2.11 °C W^{-1} for DI water. Mostafa et al. [7] studied the thermal performance of sintered wick cylindrical heat pipe with 90° bend in the condenser section. Al_2O_3/water nanofluid was used with mass fractions 1 and 3%. The average particle size was 35 nm, and the maximum input power applied was 60 W. They got lower thermal resistance for nanofluid compared with base fluid, and the evaporator wall temperature was marginally lower for 3% concentration. The effect of Al_2O_3/water nanofluid with two mass concentrations of 5 and 10% in mesh wick heat pipe was investigated by Ghanbarpour et al. [8]. The length and diameter of the heat pipe were, respectively, 200 mm and 6.35 mm. Better thermal performance was obtained for 5% concentration with an effective thermal conductivity improvement of 30%.

Surfactant-free Cu/DI water nanofluid was used in cylindrical heat pipe with stainless steel mesh wick by Kole and Dey [9] to understand the effect of particle concentration and orientation on heat pipe performance. The average particle size and the maximum input power were, respectively, 40 nm and 100 W. Various mass percentages (0.0005, 0.005, 0.05 and 0.5%) were considered, and they got best performance with 0.5% with a maximum enhancement in thermal conductivity of 15% and an average reduction in evaporator wall temperature of 14 °C. Shukla et al. [10] used cylindrical copper heat pipe of 19.5 mm diameter with DI water, Ag/DI water and Cu/DI water nanofluids. The heat input was varied from 100 to 250 W. The mass fractions were 0.008 and 0.1% for Ag/DI water and Cu/DI water nanofluids, respectively, and the corresponding enhancement in thermal efficiency was 8 and 14%. They also found a reduction of 3–27 °C in the evaporator wall temperatures due to the addition of nanoparticles.

Venkatachalapathy et al. [11] used 330-mm-long and 12-mm-outer-diameter copper mesh wick cylindrical heat pipe with CuO/DI water nanofluids with three mass fractions of 0.5, 1.0 and 1.5% in their study. The tilt angles and the input power were varied. The maximum observed reduction in thermal resistance and evaporator surface temperature was, respectively, 26.88% and 15.3 °C for 60° tilt when compared with the results of horizontal heat pipe. Thermal efficiency was found to increase with applied heat load with a maximum enhancement of 32.9 at 140 W compared with 20 W heat load. Performance of sintered wick heat pipes using CuO/DI water nanofluid was explored by Kumaresan et al. [12]. Heat input, tilt angles and mass fractions of nanofluids were varied. The optimum mass fraction and tilt angle obtained were 1.0% and 45°, respectively, and the maximum improvement in thermal efficiency was 24.9% when compared with DI water. A temperature difference of 5.1 °C was observed in the evaporator section between the wall and vapor core. Reduction in thermal resistance and increase in thermal conductivity and thermal efficiency were reported using CuO nanofluid. The effect of gold nanoparticles on the thermal performance of mesh wick heat pipe of circular cross section was investigated by Tsai et al. [13]. The heat

pipe was oriented vertically, and they found that the thermal resistance varies with the size of nanoparticles and was in the range of 0.17–0.215 °C W^{-1}.

Sadeghinezhad et al. [14] experimentally investigated sintered wick heat pipe using aqueous graphene nanoplatelets (GNP) nanofluids with various concentrations and tilt angles. The optimum concentration was found to be 0.1 mass%, and tilt angle was 60°. The maximum reduction in thermal resistance at these optimum conditions was 48.4% in comparison with DI water. The enhancement in effective thermal conductivity was 37.2% at 60 W heat input compared with horizontal position. The deposition of GNP on the wick surface in the evaporator section improved the surface wettability and thus the heat transfer rate. The effect of hybrid nanofluids on the heat transport capacity of copper mesh wick heat pipe was studied by Ramachandran et al. [15]. Al$_2$O$_3$/DI water and CuO/DI water nanofluids with three different concentrations were mixed to prepare the hybrid nanofluids. A maximum reduction of 44.25% in thermal resistance was obtained using 25–75% hybrid nanofluid compared with DI water. Experiments were conducted by Grab et al. [16] to understand the performance of thermosiphon heat pipe using TiO$_2$/DI water and Au/DI water nanofluids with two different concentrations. The addition of nanoparticles decreased the thermal resistance. The reduction in thermal resistance was 20 and 12%, respectively, for Au/DI water and TiO$_2$/DI water nanofluids. They concluded that only a small fraction of suspended nanoparticles carried by vapor to the condenser section. Wang et al. [17] studied the effect of inclination angle and operating temperature on the performance of mesh wick heat pipes using CuO nanofluids. The concentration was varied from 0.5 to 2.0 mass%, and maximum performance was obtained with 1.0 mass%. They reported that inclination has significant effect on evaporator wall temperature with minimum value at 45° tilt angle. The evaporator and condenser HTC increased 22% and 5%, respectively, as compared with horizontal orientation of heat pipe.

The effect of Ag/DI water nanofluid on the performance of mesh wick heat pipe in the horizontal mode of operation was investigated by Asirvatham et al. [18]. Three different volume concentrations of 0.003, 0.006 and 0.009% were considered. The authors reported 76.2% reduction in thermal resistance and 52.7% improvement in evaporation heat transfer coefficient for 0.009% of nanofluid. The operating range of the heat pipe was also enhanced by 21% compared with base fluid. Thermal performance of mesh wick heat pipes using ZnO/EG nanofluid was experimentally investigated by Saleh et al. [19] with volume concentrations 0.025–0.5%. They concluded that the improvement in thermal conductivity was in the range of 5.3–15.5% with respect to the base fluid and showed a nonlinear relationship with volume fraction. Experiments were performed by Mozumder

et al. [20] to find the effect of fill ratios on the performance of cylindrical heat pipes using water, methanol and acetone as working fluids. The selected fill ratios for the study were 35, 55, 85 and 100%. Fill ratios more than 85% showed a decrease in thermal resistance and an increase in heat transfer rates for all the working fluids. A review was made on the applications of nanofluids in heat pipes by Kumaresan and Venkatachalapathy [21] and summarized the effect of different nanoparticle-base fluid combinations on the thermal performance of various types of heat pipes and operating conditions. Results showed that nanoparticles dispersed in the base fluid exhibit better thermal performance than the base fluid alone.

In their critical review, Cacua et al. [22] explained that earlier nanoparticle aggregation and sedimentation adversely affect the reliable performance of heat pipes. Gupta et al. [23] used TiO$_2$-coated mesh wick and heavier TiO$_2$ nanoparticles in DI water as the working fluid in their studies. Heavier nanoparticle suspensions may produce inconsistent device thermal performance over a period of time. Moreover, from the stability point of view, the lighter the nanoparticles, the more stable the nanofluid. The thermophysical properties and stability of nanofluids are subjected to change during the operation of heat pipes due to the changes in applied thermal loads and associated phase changes. Hence, the device reliability depends more on nanofluid stability. Nanofluid technology is not fully developed and requires extensive experimental analysis to evaluate the performance of nanofluid driven heat pipes [24]. Khalid et al. [25] reviewed various factors affecting thermal performance enhancement of heat pipes such as use of nanofluid, treatment of the inner surface and use of wicks.

It was well established from the literature that the addition of nanoparticles improves the thermal performance of heat pipe. However, the existing trend of selecting the heavier metallic/metal oxide particles (Al$_2$O$_3$, TiO$_2$, CuO, etc.) in the preparation of nanofluids poses stability issues in the long run and hence affects the service life of heat pipes. Hence, the nanofluid preparation with less-density and good-thermal-conductivity particles improves the thermal diffusivity of the nanoparticle which in turn promotes faster heat transfer rates. But only limited information is available in the literature using these combinations. An agglomeration-free nanofluid suspension is a significant factor influencing the thermal performance of a heat pipe. The physical methods of achieving stability are preferred over chemical methods, as the latter method may adversely affect the thermal transport properties of the nanofluid. One of the physical methods of imparting the stability is reducing the density difference between the base fluid and nanoparticle. Jyothisankar et al. [26] attempted this approach to check the suitability of graphite–DI water nanofluid for heat transfer applications using copper mesh wick heat pipe, and the investigation was

restricted to uncoated mesh wick. However, the present work is different from the above-mentioned work, as it evaluates the thermal performance of TiO$_2$-coated copper mesh wick in a cylindrical heat pipe with graphite nanofluid at various nanoparticle concentrations, inclinations and power levels. In their review, Nazari et al. [27] reported the use of nanofluids in heat pipes and explained the role of crucial parameters such as type of nanoparticle, concentration and the stability on the successful performance of heat pipes. The objective of this study is to provide a better understanding of these crucial parameters on device level thermal performance and to demonstrate the benefits derived from seeding DI water with lighter graphite nanoparticles. This study aims to investigate the effectiveness of graphite nanofluid in hydrophilic coated mesh wick heat pipes and to confirm their improved performance.

Experimentation

Preparation of nanofluid

Graphite nanoparticles used in this study are of laboratory grade (carbon 87%) from Sisco Research Lab (SRL), India, and the base fluid is deionized water. The nanoparticles are spherical in shape with an average particle size of 10 nm. The density of the graphite sample varies from 1.2 to 2 g cc^{-1}, and specific surface area is 660–720 m^2 g^{-1}. The mass fraction of the sample is calculated using the formula,

$$mass\ fraction(\%) = \frac{m_{np}}{m_{np} + m_{bf}} \qquad (1)$$

where m_{np} and m_{bf} indicate mass of nanoparticles and base fluid, respectively.

The mass of the nanoparticle and the DI water is measured using a precision electronic balance and are mixed together to prepare the nanofluid samples at three different mass fractions, viz. 0.5, 1.0 and 1.5%. The conventional two-step method is followed for the preparation of nanofluid, and no surfactant or dispersant is used. The addition of surfactants or dispersants affects the thermal conductivity and capillarity of the nanofluid and thus the heat pipe performance; they are not used in this study. Stable and even suspension of graphite nanoparticles in DI water is achieved by intense magnetic stirring with 0.5 and 1.0 mass% samples at 1700 rpm while 1.5 mass% sample at 2000 rpm. This is followed by ultrasonication at the frequency of 40 kHz using an ultrasonic bath. The prepared nanofluid is kept for 3 weeks for physical examination in order to confirm the stability of the suspension. There are no visible traces of sedimentation found during this time frame. Figure 1 shows
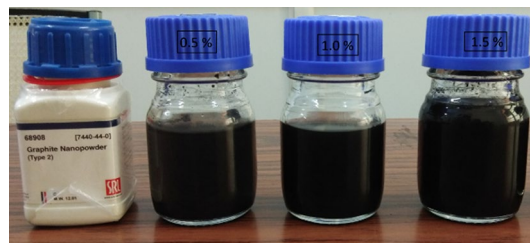
Fig. 1 Nanofluid Samples after 21 days

the prepared nanofluids after 21 days, and this confirms its stability. A small amount of sedimentation is observed for 1.5% particle loading after 80 days.

The main reason for selecting the graphite nanoparticle in this work is its comparatively low density and high thermal diffusivity. Also, the low density imparts further stability to the prepared suspension. The stability of the sample is confirmed by measuring the Zeta potential (Malvern Instrument, UK), and the measured values are 36.9, 35.8 and 33.5 mV for 0.5, 1.0 and 1.5 mass%, respectively. The Zeta potential distribution for 1.0% concentration shows a single observed peak as depicted in Fig. 2. The magnitude of Zeta potential is an indication of suspension stability; a value greater than 30 mV indicates a good degree of stability. The Zetasizer data show that graphite nanoparticles remain dispersed in the fluid with average diameter less than 176 nm. The shape, size and state of agglomeration of the graphite nanoparticles are examined using transmission electron microscope (TEM). Figure 3 shows the TEM image of graphite–DI water nanofluid taken after 50 days for 1.0 mass%. The TEM image points out that the graphite nanoparticles have spherical morphology and also a slight agglomeration of the nanoparticles. Slight agglomeration is observed with 1.5 mass% sample also mainly due to higher particle loading.

Properties of nanofluid

The thermophysical properties of the prepared nanofluid samples are experimentally measured with the help of various instruments, and the values are given in Table 1. KD2 PRO Thermal Properties Analyzer (Decagon Devices, USA) based on the principle of transient hot wire method is used to measure the thermal conductivity of nanofluids. The measured values show an increase in the thermal conductivity with particle loading. The improvement in thermal conductivity is 3.5, 22 and 38% for 0.5, 1.0 and 1.5 mass % particle loading in comparison with DI water. The surface tension of the samples is measured at 27 °C and 60% relative humidity using Holmarc Goniometer, which is based on sessile liquid drop method. Initially, DI water is tested and the value obtained is in close agreement with those available in the literature. A maximum increment of 3% is obtained for

Fig. 2 Zeta potential for 1.0 mass% sample after 21 days
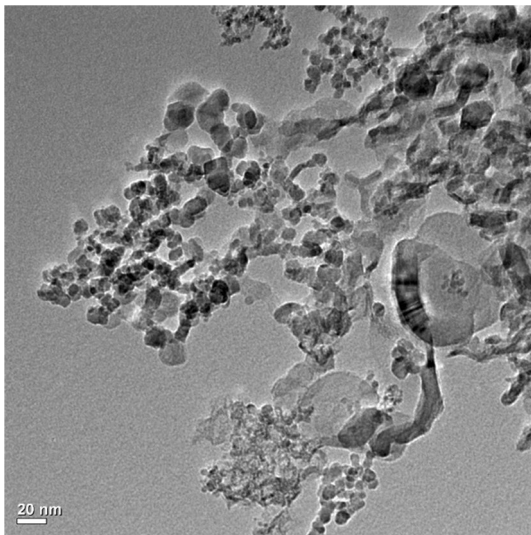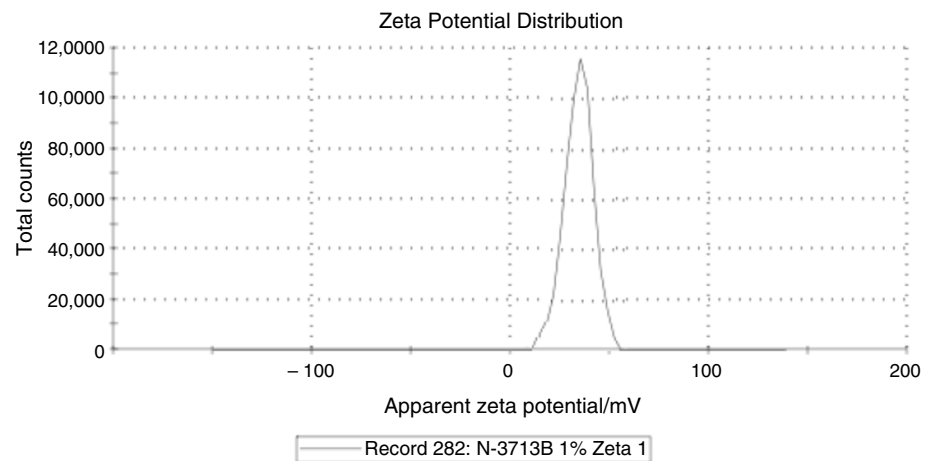
Fig. 3 TEM image of graphite–DI water nanofluid after 50 days (1.0% concentration)

the highest particle loading when compared with DI water. Brooke Field Viscometer (DV-E, version 1.10) is used to measure the dynamic viscosity, and the measured values show a nonlinear increase in viscosity with particle loading and for 1.5 mass%; it is twice that of DI water. The

instrument accuracy reported by the manufacturer is ±1%. In summary, the thermophysical properties of nanofluid samples are strong functions of particle loading.

For the effective functioning of heat pipes, working fluid must be compatible with the wick structure. Also, the wettability of the wick structure with the working fluid is essential and is quantified by the contact angle. Wettability indicates that the fluid must spread over the wick structure or always keeps the wick to be saturated. With water as working fluid, a contact angle less than 90° is termed as hydrophilic and that greater than 90° is termed as hydrophobic. The contact angle of the prepared graphite nanofluid is greater than that of the base fluid. This may affect the performance of a heat pipe, even though the graphite nanofluid possesses good thermophysical properties. In order to reduce the contact angle, it is decided to make a hydrophilic coating of TiO_2 over the wick structure. A carefully prepared solution containing tetrabutyl orthotitanate, diethanolamine, ethanol and polyethylene glycol is vigorously stirred in a magnetic stirrer for 4 h. The wick is dipped in this solution, air-dried and then sintered in an oven to get the hydrophilic coating, as mentioned by Jyothisankar et al. [28]. The coated wick is finally washed with tap water to ascertain the bonding of TiO_2 coating over the wick. The coating lowers the contact angle by 20° for 0.5% sample to 35° for 1.5% sample. KRUSS Liquid Drop Analyzer is used for the measurement

Table 1 Thermophysical properties of the nanofluid

Sample	Thermal conductivity/W m^{-1} K^{-1}		Surface tension/mN m^{-1}		Viscosity/mPa s	
	Measured value	Uncertainty (5%)	Measured value	Uncertainty (3%)	Measured value	Uncertainty (1%)
DI water	0.59	±0.0295	72.0	±2.160	1.0	±0.010
0.5% sample	0.61	±0.0305	72.5	±2.175	1.0	±0.010
1.0% sample	0.72	±0.0360	73.2	±2.196	1.2	±0.012
1.5% sample	0.81	±0.0405	74.2	±2.226	2.0	±0.020

of contact angle, and the values are given in Table 2 for bare and coated mesh wick. With increasing particle loading, the contact angle increases. However, it decreases with TiO_2 coating, with a maximum reduction at 1.5 mass%.

Experimental setup

The schematic diagram of the heat pipe with thermocouple positions is shown in Fig. 4. The heat pipe is fabricated from a plain copper cylindrical tube of outer diameter 12 mm, wall thickness 0.5 mm and length 300 mm. Three layers of TiO_2-coated copper mesh wick (100 mesh $inch^{-1}$) are rolled and inserted into the copper tube. Each end of the copper tube is closed with a 3-mm-thick copper end cap. The entire length of the heat pipe is divided into three length zones; first, 90 mm is the evaporator zone followed by a 75 mm of adiabatic zone and finally a 135 mm of condenser zone. A total of 14 calibrated T-type thermocouples with a measurement accuracy of ± 0.5 °C are used in the setup. Six thermocouples are used to measure the vapor temperature, denoted by V_1 through V_6 and the remaining six for wall temperatures designated by W_1 through W_6. The symmetrical placement of thermocouples enables to figure out the temperature profiles on each zone. The entire section of the evaporator is covered with electrically insulating and thermally conducting mica

Table 2 Contact angle measurement

Sample	Type of surface	Contact angle (°)
Base fluid	Bare copper	91.3
	TiO_2 coated	68.6
0.5 mass%	Bare copper	96.6
	TiO_2 coated	77.0
1.0 mass%	Bare copper	100.8
	TiO_2 coated	78.0
1.5 mass %	Bare copper	114.9
	TiO_2 coated	79.1

sheet. An autotransformer supplies regulated power to the circumferential heater, and the power input to the evaporator is calculated from the digital multimeter. Glass wool insulation of thickness 50 mm is provided in the entire evaporator zone to minimize the heat loss to the ambient. The adiabatic zone is also covered with glass wool insulation. Heat is removed from the condenser zone by circulating cold water from the chiller unit which supplies cold water in the range 18–20 °C. An acrylic cylinder of 32 mm diameter and 150 mm length is mounted around the condenser zone over its entire length so as to keep it always submerged in a pool of cold water. A rotameter measures the flow rate of the cooling water. Two T-type thermocouples are used, one each in the inlet and outlet of condenser section to measure the temperature of the circulating cold water. The schematic diagram of the experimental setup is shown in Fig. 5. The heat pipe is charged with 90% of the evaporator volume which is about 8.3 mL of nanofluid. This quantity is sufficient to completely saturate the mesh wick structure.
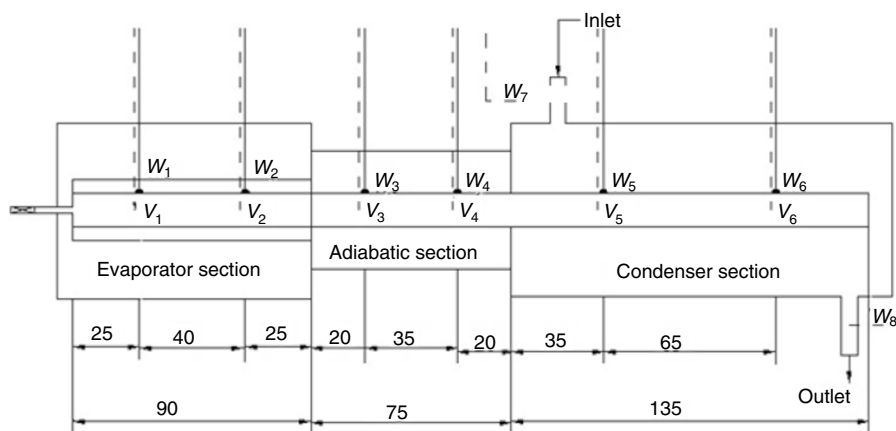
Experimental procedure

Four identical heat pipes are considered in this study. One heat pipe uses uncoated (UCW) mesh wick with DI water as working fluid. The other three hydrophilic TiO_2-coated (CW) mesh wick heat pipes are filled with graphite—DI water nanofluid at three different mass concentrations, viz. 0.5, 1.0 and 1.5%. The heat energy supplied at the evaporator is in steps of 30 W, ranging from 30 to 180 W, and the corresponding heat fluxes range is 8.8–53.1 kW m^{-2}. The maximum input power is restricted to either burn out of the heat pipe or the maximum operating temperature of 120 °C found on the evaporator wall. The experiments are repeated for different inclinations of the heat pipe starting from 0° or horizontal, 30, 45, 60 and 90° or vertical. For all the inclination angles, the evaporator section is always kept below the condenser section. All the temperature signals are scanned at 30-s interval by an Agilent Data Logger and
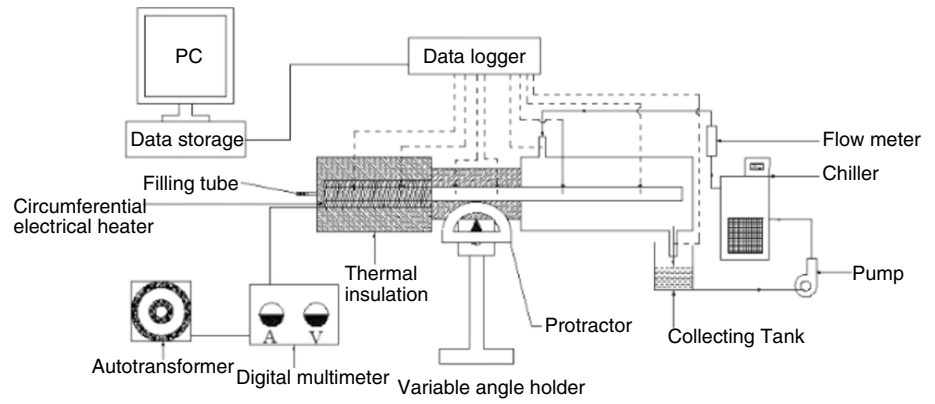
Fig. 4 Thermocouple positions on heat pipe (all dimensions are in mm)

Fig. 5 Schematic diagram of the experimental setup

stored in a personal computer. In this analysis, steady state was normally achieved at the end of 30 min for most of the cases and the criterion for a steady state was a difference of less than 1 °C in adiabatic wall temperature for 3 min. The steady-state values of the temperatures are picked up for further data reduction.

Data reduction

The heat pipe transfers heat energy from evaporator end to condenser end. Difference in the average wall temperatures between these two sections of the heat pipe is called overall temperature difference (ΔT_o).

$$\Delta T_o = \overline{T}_{ew} - \overline{T}_{cw} \tag{2}$$

On the experimental arrangement as shown, each section of the heat pipe is monitored with four thermocouples, two each for wall and vapor core. So the average temperatures are given by

$$\overline{T}_{ew} = \frac{T_{w1} + T_{w2}}{2} \tag{3}$$

$$\overline{T}_{ev} = \frac{T_{v1} + T_{v2}}{2} \tag{4}$$

$$\overline{T}_{cw} = \frac{T_{w5} + T_{w6}}{2} \tag{5}$$

$$\overline{T}_{cv} = \frac{T_{v5} + T_{v6}}{2} \tag{6}$$

where $\overline{T}_{ew}$, $\overline{T}_{ev}$, $\overline{T}_{cw}$ and $\overline{T}_{cv}$ represent the average values of temperature for the evaporator wall, evaporator vapor core, condenser wall and condenser vapor core, respectively. The temperature difference at the vapor core area is given by,

$$\Delta T_v = \overline{T}_{ev} - \overline{T}_{cv} \tag{7}$$

Heat input to the heat pipe is calculated from the ammeter (I) and voltmeter (V) readings.

$$Q = V \cdot I \tag{8}$$

Heat taken away by the circulating cold water is calculated using the following equation:

$$Q_c = \dot{m}_w C_{pw} \Delta T_w \tag{9}$$

where $\dot{m}_w$ is the mass flow rate of cooling water through the condenser, ΔT_w is the rise in temperature, and C_{pw} is the specific heat capacity.

Thermal efficiency of the heat pipe is the ratio of heat rejected in the condenser section to heat absorbed in the evaporator section.

$$\eta_{th} = \frac{Q_c}{Q} \tag{10}$$

Heat pipe thermal resistance is the ratio between overall temperature difference and heat input.

$$R_{th} = \frac{\Delta T_o}{Q} \tag{11}$$

Equivalent thermal conductivity of the heat pipe is calculated using the equation

$$k_{eq} = \frac{Q}{A_{cs} \cdot \Delta T_o} \tag{12}$$

where A_{cs} represents the cross-sectional area of the heat pipe.

The average heat transfer coefficient of the combined evaporator and condenser sections is given by

$$h_{av} = \frac{Q + Q_c}{A_{ec} \cdot \Delta T_o} \tag{13}$$

where A_{ec} is the sum of the surface areas of evaporator and condenser sections.

Uncertainty analysis

The uncertainties in the measurement are determined based on the method given by Kline and McClintock. Uncertainty in the heat input, heat flux, thermal resistance, heat transfer coefficient and thermal efficiency is given in Eqs. (14)–(18), respectively.

$$\frac{\Delta Q}{Q} = \left[\left(\frac{\Delta V}{V} \right)^2 + \left(\frac{\Delta I}{I} \right)^2 \right]^{\frac{1}{2}} \tag{14}$$

$$\frac{\Delta q}{q} = \left[\left(\frac{\Delta V}{V} \right)^2 + \left(\frac{\Delta I}{I} \right)^2 + \left(\frac{\Delta L}{L} \right)^2 + \left(\frac{\Delta d}{d} \right)^2 \right]^{\frac{1}{2}} \tag{15}$$

$$\frac{\Delta R}{R} = \left[\left(\frac{\Delta Q}{Q} \right)^2 + \left(\frac{\Delta (\Delta T)}{\Delta T} \right)^2 \right]^{\frac{1}{2}} \tag{16}$$

$$\frac{\Delta h}{h} = \left[\left(\frac{\Delta q}{q} \right)^2 + \left(\frac{\Delta (\Delta T)}{\Delta T} \right)^2 \right]^{\frac{1}{2}} \tag{17}$$

$$\frac{\Delta \eta}{\eta} = \left[\left(\frac{\Delta Q}{Q} \right)^2 + \left(\frac{\Delta \dot{m}_c}{\dot{m}_c} \right)^2 + \left(\frac{\Delta (\Delta T_w)}{\Delta T_w} \right)^2 \right]^{\frac{1}{2}} \tag{18}$$

Uncertainty in heat input depends on the accuracy of voltmeter and ammeter. In the case of heat flux, uncertainty depends on heat input, length and diameter measurements. For thermal efficiency, the uncertainty accounts from heat input, temperature change of cold water and its mass flow rate. The uncertainties of the derived quantities are calculated using the above-mentioned method for each operating condition. The maximum uncertainty in heat flux, thermal resistance, heat transfer coefficient and thermal efficiency is, respectively, 3.95, 4.14, 4.64 and 5.17%. Thus, the maximum uncertainty present in the calculation of any derived quantities representing the heat transfer performance of heat pipe is around 5%.

Results and discussion

Experiments are carried out for various inclinations and power inputs of the heat pipe. Throughout the study, the condenser end is kept above the evaporator end except for the horizontal mode of operation.
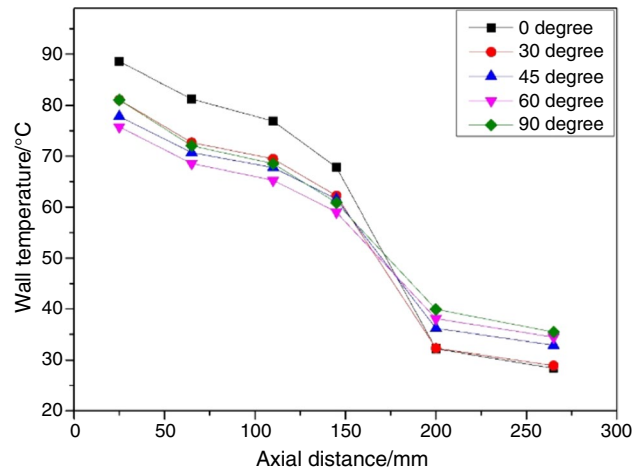

Fig. 6 Wall temperature distribution with DI water and 120 W input for various tilt angles
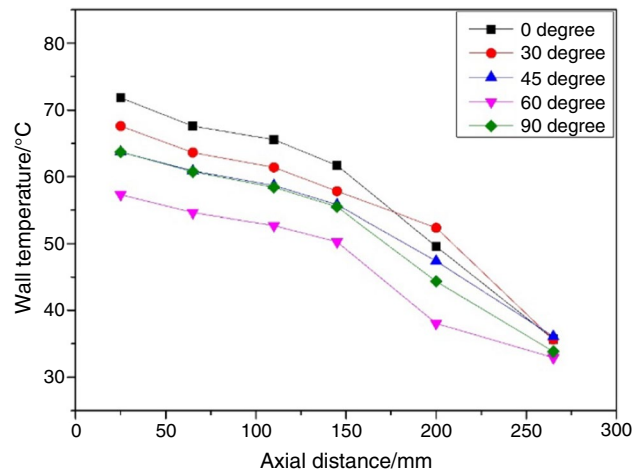

Fig. 7 Effect of tilt angle on wall temperature for 1.0 mass % sample and 120 W input power

Effect of tilt angle on axial wall temperature

Heat pipe wall temperature distribution along its length for various tilt angles portrays the elimination of noncondensable gas generation and is represented in Figs. 6 and 7. As shown in Fig. 6, the wall temperature at the evaporator section decreases with the increasing tilt angle of the heat pipe using DI water with uncoated wick. Minimum wall temperature is obtained at 60°, beyond which a moderate increase is observed. For horizontal operation, the temperature gradient is maximum at the evaporator and condenser ends compared with other tilt angles, which is due to partial dry out that may occur at several spots locally at the evaporator

section. When the heat pipe is tilted from its horizontal position gradually, the gravity helps the condensate return to the evaporator, thereby delaying the occurrence of partial dry out. The wall temperature distribution is shown in Fig. 7 for 1.0 mass% nanoparticle loading and different tilt angles. The temperature in the evaporator region decreases by the addition of nanoparticles, and 60° angular tilt gives better thermal performance compared with other tilt angles. This is because 60° angular tilt provides somewhat controlled flow of condensate return without affecting the nucleate bubbling phenomena occurring on the evaporator region for the applied heat flux. Increasing the input power to 180 W increases the evaporator wall temperature to 92.47, 79.69, 76.08, 72.47 and 77.35 °C, respectively, for the tilt angles 0, 30, 45, 60 and 90°. So heat pipe is optimized for different tilt angles, and the lowest wall temperature is observed at 60° angular tilt.

Tilt angle is one of the main parameters on which the thermal performance of a heat pipe depends on. For example, with a power input of 120 W, the associated temperature drop between the evaporator and condenser wall of DI water heat pipe is found to be 54.62 °C for horizontal and 39.73 °C for 60° tilt. Under the same input power conditions, the respective values are 27.11 and 20.50 °C for heat pipe operated with 1.0 mass % nanoparticle loading. It is seen that in both cases, the gravity significantly improved the heat pipe performance by reducing the temperature drop by 50%.

Effect of particle loading on axial wall temperature

The wall temperature variation of all samples is shown in Fig. 8 for an input power of 120 W and an inclination angle of 60°. The wall temperature for all the samples decreases from evaporator side to the condenser side, indicating the heat flow from evaporator to condenser. Maximum temperature difference between evaporator end and condenser end is observed for DI water with uncoated wick (UCW), while the lowest one is observed for 1.0 mass% of nanofluid. In the evaporator section, the reduction in wall temperature is significant due to the addition of graphite nanoparticles which in turn enhances the thermal performance of heat pipes. This is due to increased thermal conductivity and thermal diffusivity of the nanofluid in comparison with DI water. This shows the addition of nanoparticles reduces the evaporator wall temperature and hence improves the heat transfer capability of working fluid by elevating the critical heat flux [29]. However, the wall temperature for 1.5% sample is higher than 1.0% sample due to higher flow resistance caused by increased viscosity which reduces the movement of nanofluid from condenser to evaporator section. The maximum reduction obtained for 0.5, 1.0 and 1.5% samples is, respectively, 23.57, 34.08 and 28.10% compared with DI water. When the heat input is increased to 180 W, the
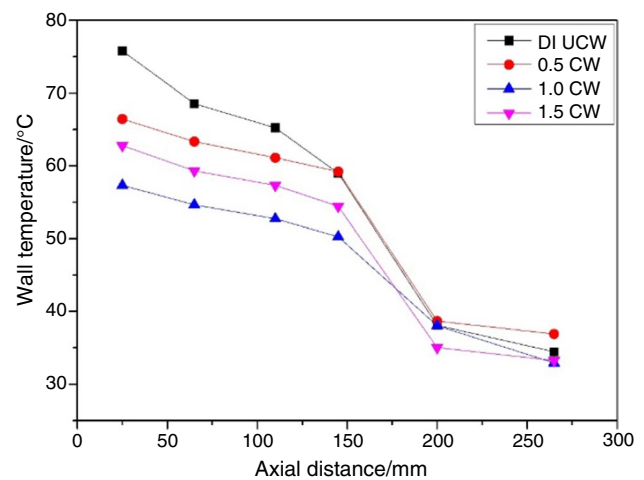

Fig. 8 Wall temperature distribution in the axial direction at 120 W heat input and 60° tilt angle

corresponding values are 21.50, 25.56 and 21.11%. Thus, the heat pipe is studied for different particle loadings and the lowest wall temperature is found with 1.0 mass% sample, which is the optimum particle loading.

Effect of particle loading on vapor temperature difference

Figure 9 represents the vapor temperature difference between evaporator and condenser sections for all concentrations at a fixed tilt angle of 60°. The temperature difference increases with heat loads. It is maximum for DI water and minimum for 1.0 mass%. For the maximum heat input, the vapor temperature difference of DI water and nanofluid heat pipes is found to be 44.51, 27.95, 21.70 and 29 °C at 60° tilt. The higher temperature difference for maximum mass fraction is due to insufficient condensate return because of higher viscosity. Vapor temperature difference indicates the performance of heat pipe, a minimum value of which exhibits the best performance. Any increase in vapor temperature at a particular heat load shows insufficient condensate return to the evaporator.

Effect of inclination on thermal resistance for various particle loading

The overall thermal resistance of heat pipe is calculated on the basis of average wall temperatures at the evaporator and condenser ends. This resistance stems from two component resistances; the first one is the resistance between evaporator and adiabatic sections, and the second is the resistance between adiabatic and condenser sections. Among these two component resistances, the major contribution is by the first one as explained by Sai et al. [13]. Orientation has strong
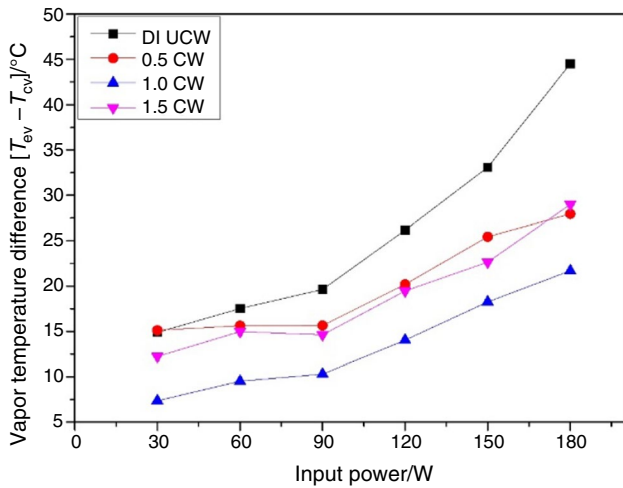
Fig. 9 Vapor temperature difference $(T_{ev} - T_{cv})$ of all samples at 60° tilt

Fig. 10 Influence of tilt angle on thermal resistance at 120 W

influence on the heat pipe performance with maximum thermal resistance at horizontal position and minimum at 60° tilt. Thermal resistance is higher at lower heat loads due to the presence of a relatively thick liquid film enveloping the evaporator section, thus increasing the conduction resistance. As the heat load increases, this film breaks up resulting in lowering of conduction resistance. This behavioral pattern of thermal resistance in response to the heat input is a common characteristic feature of heat pipes as suggested by Hopkins et al. [30].

Figure 10 depicts the overall thermal resistance variation for different concentrations at 120 W of input power. All the samples follow the characteristic behavioral pattern and the curves shifting downward indicating lower thermal resistances. Thermal resistance is found to decrease with gravity and reaches a minimum value at 60° tilt. This is because larger tilt encourages condensate flow to the evaporator and reaches an optimum resistance value at around 60°. Beyond this, the condensate return increases and forming a liquid film over the mesh surface, thereby decreasing the rate of radial heat transfer which results in increased thermal resistance. Lowest thermal resistance is obtained with 1.0 mass % sample and 60° tilt. The flow of nanofluid causes lodging of nanoparticles over the wick structure, thereby providing an extended surface for the heat transfer, improved capillarity and hence lower thermal resistance. The thermal resistances of all the concentrations are compared at a tilt angle of 60° and are presented in Fig. 11. The results suggest that the heat transport capacity of graphite nanofluid heat pipe is more than that of DI water-based heat pipe due to reduced thermal resistance.

Effect of particle loading on thermal efficiency

Thermal efficiency is an important parameter for quantifying the heat pipe performance as it estimates the amount of heat
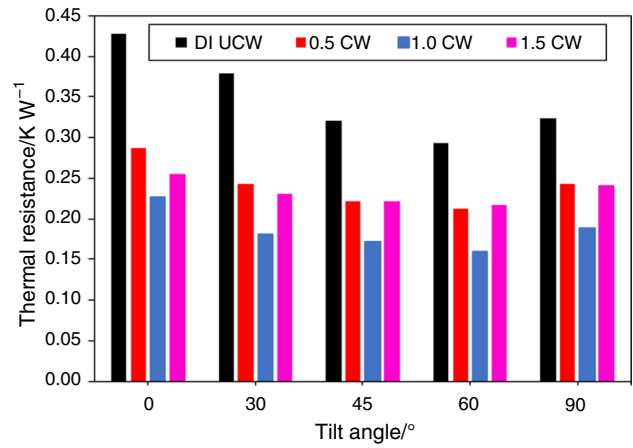
absorbed in the evaporator section. Thermal efficiency of all the samples is plotted in Fig. 12. The thermal efficiency is in a direct relationship with heat load for all nanofluid concentrations. It increases with heat loads as thermal resistance is lower at higher heat loads. At 120 W of operation, the 1.0 mass% nanofluid at optimum tilt attains a thermal efficiency of 93.18% compared to 75.16% of DI water at the same tilt. Efficiency increases with particle loading; however, the high viscosity of the 1.5 mass% sample delays liquid flow along the wick structure to the evaporator, thereby causing slight reduction of it. The efficiency of DI water heat pipe decreases for heat inputs beyond 120 W, indicating the occurrence of partial dry out. The potential factors affecting the thermal efficiency are the heat pipe orientation and thermophysical properties of the working fluid.

Effect of particle loading on equivalent thermal conductivity

The effect of particle loading and applied heat flux on the heat transport capacity of the heat pipe, measured in terms of equivalent thermal conductivity, is shown in Fig. 13. The thermal conductivity of all heat pipes increases
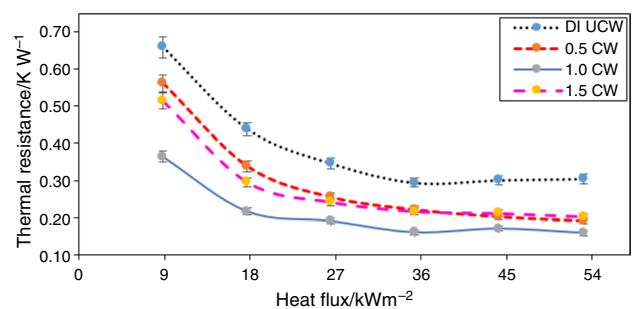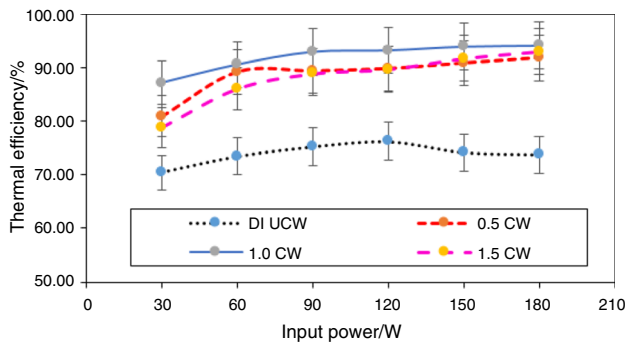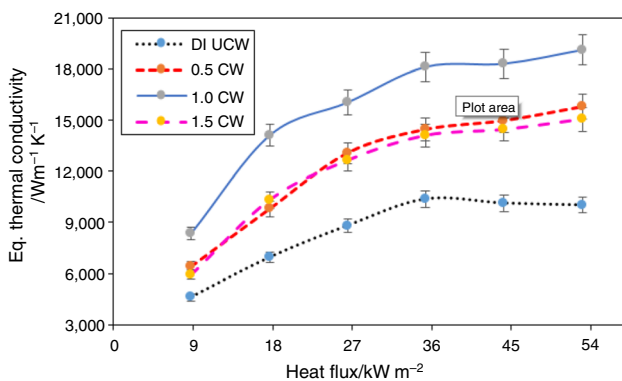

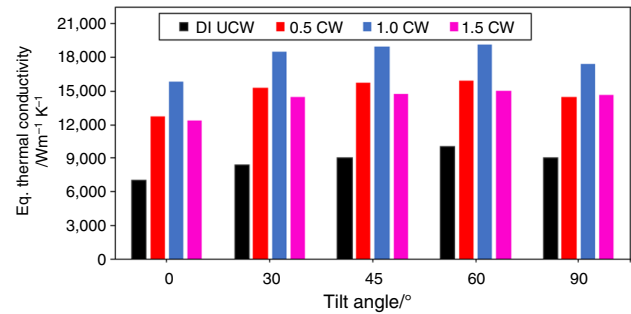Fig. 11 Thermal resistance for all concentrations at 60° tilt angle

Fig. 12 Thermal efficiency of the heat pipe for all samples at 60° tilt angle
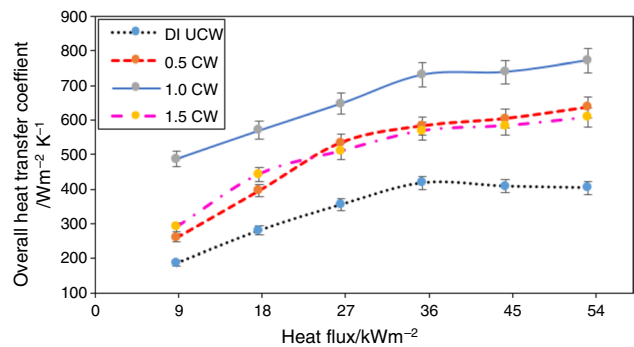

Fig. 14 Equivalent thermal conductivity at all concentrations and 180 W heat input

Fig. 13 Equivalent thermal conductivity at all concentrations and 60° tilt angle

Fig. 15 Overall heat transfer coefficient of all samples at 60° tilt

with heat flux irrespective of heat pipe orientation. The maximum effective thermal conductivity is found out for 1.0% mass fraction of graphite nanofluid, whose value is 19.11 kW m^{-1} K^{-1} at a flux of 53.1 kW m^{-2}. The maximum values obtained for 0.5, 1.0 and 1.5% samples are, respectively, 59.08, 90.87 and 50.18% compared with DI water at the optimum tilt. The addition of higher conducting graphite nanoparticles enhances the equivalent thermal conductivity. Formation of thin nanoparticle coating over the wick surface due to the movement of nanofluid also increases thermal conductivity. However, decrement occurs at the highest mass fraction due to increased viscosity of nanofluid. The equivalent thermal conductivity of all samples at 180 W input and various tilt angles is shown in Fig. 14. Orientation of the heat pipe affects the equivalent thermal conductivity with the lowest value in horizontal position, increases up to 60° and decreases afterward. This is because the faster condensate return at higher angle of tilts delays the vapor generation at the evaporator in accordance with heat flux crept in.

Effect of particle loading on overall heat transfer coefficient

Figure 15 shows average heat transfer coefficient of all samples at 60° tilts. The heat transfer coefficient increases with angle of tilt, and it reaches the optimum value around a tilt angle of 60°. Beyond that, it marginally decreased due to the small reduction on the heat transfer on the evaporator due to the quicker condensate return. The observed maximum enhancement of heat transfer coefficient was found to be 57.45, 90.87 and 50.19% for three mass fractions, namely 0.5, 1.0 and 1.5%, respectively, when compared to DI water. The heat transfer coefficient depends on both tilt angle and mass fractions of the nanoparticle. With the addition of nanoparticle, the Brownian motion of the nanoparticle in the suspension improves. As the temperature of working fluid increases due to the addition of heat flux, Brownian motion also increases which in turn increases the convective heat transfer of the nanofluid. So heat transfer coefficient increases with heat flux.

Repeatability test and performance stability

Equivalent thermal conductivity is one of the main parameters used to judge the thermal performance of heat pipes.

Repeatability chart
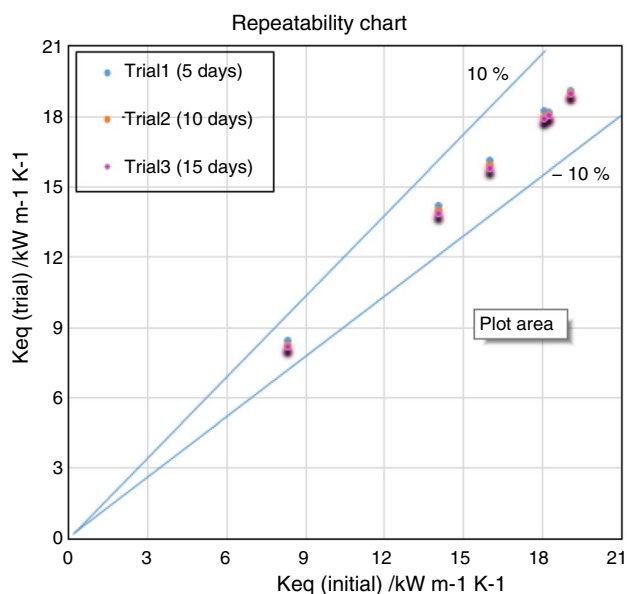
Fig. 16 Repeatability and performance stability test of 1.0 mass% samples at 60° tilt

The adhesiveness of hydrophilic coating over the wick must be ensured for the satisfactory functioning of heat pipes. To ensure the performance stability, a repeatability test is conducted with equivalent thermal conductivity as a parameter at the end 5th, 10th and 15th days in three trials. Figure 16 shows the results of a repeatability test done with each trial consisting of input power varying from 30 to 180 W. The 1.0 mass percentage particle loading sample is taken for the case study, and maximum variation is found to be within 2.92%. This confirms that the hydrophilic coating over the wick is stable and results are repeatable even after the applied heat load up to 180 W.

Effect of input flux on evaporator wall temperature distribution

The evaporator wall temperature is the primary data for estimating the performance of heat pipe. The present work is compared with Liu et al. [31]. They reported the axial temperature distributions using both deionized water and CuO nanofluid for a heat flux of 9.61 kW m^{-2} and a concentration of 1.0 mass%. The evaporator wall temperatures using nanofluid are found to be much lower than that of DI water for the same heat flux. They found the optimum concentration as 1.0 mass% and claimed a significant reduction in the evaporator wall temperature. Consequently, the heat transfer efficiency of the heat pipe was greatly improved. From our studies, it is observed that the evaporator wall temperature with base fluid increases significantly with the thermal loads. However, addition of nanoparticles lowers the evaporator wall temperatures. The present analysis of graphite/DI water nanofluid

gives an evaporator surface temperature of 69.7 °C at a heat flux of 35.3 kW m^{-2} in the horizontal mode. For the same orientation, the corresponding values reported by Liu et al. [31] were 68 °C at 9.61 kW m^{-2}, respectively. The higher flux handling capacity in the present study is attributed to the high thermal diffusivity of the graphite nanoparticle and hence better boiling heat transfer in the evaporator region.

Conclusions

The thermal performance of mesh wick heat pipes using graphite–DI water nanofluid with three mass fractions is experimentally investigated. Axial wall temperature distribution, vapor temperature drop, thermal resistance, thermal efficiency and equivalent thermal conductivity are evaluated, and the results are compared with heat pipe using DI water. The results reveal better performance for nanofluid charged heat pipes owing to the favorable thermophysical properties of graphite–DI water nanofluid. Graphite nanoparticles dispersion in base fluid is more stable than copper nanoparticle dispersion and also improves the thermal conductivity as well as convective heat transfer due to Brownian motion. Further, higher thermal diffusivity of graphite nanoparticle quickens the heat transfer and facilitates the vaporization of base fluid. The mass fractions as well as tilt angles have significant effect on the evaporator wall temperature reduction and push up the operating limits of heat pipe. Angle of inclination facilitates faster condensate return to the evaporator. However, at larger inclinations (more than 60°), the quicker condensate returns affects the vapor–liquid flow dynamics in the evaporator zone, resulting in deterioration of performance. Particle loading of 1.0 mass% and a tilt angle of 60° are more efficient. Thermal resistance decreases from 0.43 K W^{-1} for horizontal mode with DI water and uncoated wick to 0.16 K W^{-1} for mass concentration 1.0% and 60° tilt. The maximum values of equivalent thermal conductivity and thermal efficiency are, respectively, 19.11 kW m^{-1} K^{-1} and 94.07% at this concentration and tilt angle. The enhanced thermal performance showcases graphite nanofluid as an attractive working fluid for mesh wick heat pipes.

References

1. Bejan A, Kraus AD. Heat Transfer Hand Book. New York: Wiley; 2003.

2. Faghri Amir, Guo Zhen. Integration of heat pipe into fuel cell technology. Heat Transf Eng. 2008;29:232–8.

3. Guo Qing, Guo Hang, Yan XK, Ye Fang, Ma CF. Influence of inclination angle on the start-up performance of a sodium-potassium alloy heat pipe. Heat Transf Eng. 2017. https://doi.org/10.1080/01457632.2017.1370325.

4. Cheng Lixin, Xia Guodong, Li Qinling, Thome John R. Fundamental issues, technology development and challenges of boiling heat transfer, critical heat flux and two-phase flow phenomena with nanofluids. Heat Transf Eng. 2018. https://doi.org/10.1080/01457632.2018.1470285.

5. Buongiorno J, Venerus DC, Prabhat N, McKrell T, Townsend J, Christianson R, Tolmachev YV, Keblinski P, Hu LW, Alvarado JL, Bang IC, Bishnoi SW, Bonetti M, Botz F, Cecere A, Chang Y, Chen G, Chen H, Chung SJ, Chyu MK, Das SK, Paola RD, Ding Y, Dubois F, Dzido G, Eapen J, Escher W, Funfschilling D, Galand Q, Gao J, Gharagozloo PE, Goodson KE, Gutierrez JG, Hong H, Horton M, Iorio CS, Jarzêbski AB, Jiang Y, Jin LW, Kabelac S, Kamath A, Kedzierski MA, Kim C, Kim JH, Kim S, Kieng LG, Leong KC, Manna I, Michel B, Ni R, Patel HE, Philip J, Poulikakos D, Reynaud C, Savino R, Singh PK, Song P, Sundararajan T, Timofeeva E, Tritcak T, Turanov AN, Vaerenbergh SV, Wen D, Witharana S, Yang CC, Yeh WH, Zhao XZ, Zhou SQ. A benchmark study on the thermal conductivity of nanofluids. J Appl Phys. 2009;106:094312. https://doi.org/10.1063/1.3245330.

6. Putra N, Septiadi WN, Rahman H, Irwansyah R. Thermal performance of screen mesh wick heat pipes with nanofluids. Exp Therm Fluid Sci. 2012;40:10–7. https://doi.org/10.1016/j.expthermflusci.2012.01.007.

7. Moraveji MK, Razvarz S. Experimental investigation of aluminum oxide nanofluid on heat pipe thermal performance. Int Commun Heat Mass Transf. 2012;39:1444–8. https://doi.org/10.1016/j.icheatmasstransfer.2012.07.024.

8. Ghanbarpour M, Nikkam N, Khodabandeh R, Toprak MS, Muhammed M. Thermal performance of screen mesh heat pipe with Al_2O_3 nanofluid. Exp Therm Fluid Sci. 2015;66:213–20. https://doi.org/10.1016/j.expthermflusci.2015.03.024.

9. Kole M, Dey TK. Thermal performance of screen mesh wick heat pipes using water-based copper nanofluids. Appl Therm Eng. 2013;50:763–70. https://doi.org/10.1016/j.applthermaleng.2012.06.049.

10. Shukla KN, Solomon AB, Pillai BC, Ibrahim M. Thermal performance of cylindrical heat pipe using nanofluids. J Thermophys Heat Transf. 2010;24:796–802. https://doi.org/10.2514/1.48749.

11. Venkatachalapathy S, Kumaresan G, Suresh S. Performance analysis of cylindrical heat pipe using nanofluids—an experimental study. Int J Multiph Flow. 2015;72:188–97. https://doi.org/10.1016/j.ijmultiphaseflow.2015.02.006.

12. Kumaresan G, Venkatachalapathy S, Asirvatham LG. Experimental investigation on enhancement in thermal characteristics of sintered wick heat pipe using CuO nanofluids. Int J Heat Mass Transf. 2014;72:507–16. https://doi.org/10.1016/j.ijheatmasstransfer.2014.01.029.

13. Tsai CY, Chien HT, Ding PP, Chan B, Luh TY, Chen PH. Effect of structural character of gold nanoparticles in nanofluid on heat pipe thermal performance. Mater Lett. 2004;58:1461–5. https://doi.org/10.1016/j.matlet.2003.10.009.

14. Sadeghinezhad E, Mehrali M, Rosen MA, Akhiani AR, Latibari ST, Mehrali M, Metselaar HSC. Experimental investigation of the effect of graphene nanofluids on heat pipe thermal performance. Appl Therm Eng. 2016;100:775–87. https://doi.org/10.1016/j.applthermaleng.2016.02.071.

15. Ramachandran R, Ganesan K, Rajkumar MR, Asirvatham LG, Wongwises S. Comparative study of the effect of hybrid nanoparticle on the thermal performance of cylindrical screen mesh heat pipe. Int Commun Heat Mass Transf. 2016;76:294–300. https://doi.org/10.1016/j.icheatmasstransfer.2016.05.030.

16. Grab T, Gross U, Franzke U, Buschmann MH. Operation performance of thermosyphons employing titania and gold nanofluids. Int J Therm Sci. 2014;86:352–64. https://doi.org/10.1016/j.ijthermalsci.2014.06.019.

17. Wang PY, Chen XJ, Liu ZH, Liu YP. Application of nanofluid in an inclined mesh wicked heat pipes. Thermochim Acta. 2012;539:100–8. https://doi.org/10.1016/j.tca.2012.04.011.

18. Asirvatham LG, Nimmagadda R, Wongwises S. Heat transfer performance of screen mesh wick heat pipes using silver–water nanofluid. Int J Heat Mass Transf. 2013;60:201–9. https://doi.org/10.1016/j.ijheatmasstransfer.2012.11.037.

19. Saleh R, Putra N, Prakoso SP, Septiadi WN. Experimental investigation of thermal conductivity and heat pipe thermal performance of ZnO nanofluids. Int J Therm Sci. 2013;63:125–32. https://doi.org/10.1016/j.ijthermalsci.2012.07.011.

20. Mozumder AK, Akon AF, Chowdhury MSH, Banik SC. Performance of heat pipe for different working fluids and fill ratios. J Mech Eng. 2010;41:96–102.

21. Kumaresan G, Venkatachalapathy S. A review on heat transfer enhancement studies of heat pipes using nanofluids. Front Heat pipes. 2012. https://doi.org/10.5098/fhp.V3.4.3001.

22. Cacua K, Buitrago-Sierra R, Herrera B, Pabon E, Murshed SMS. Nanofluids' stability effects on the thermal performance of heat pipes. J Therm Anal Calorim. 2019;136:1597–614. https://doi.org/10.1007/s10973-018-7787-5.

23. Gupta NK, Tiwari AK, Ghosh SK. Experimental study of thermal performance of nanofluid-filled and nanoparticles-coated mesh wick heat pipes. J Heat Transf. 2018. https://doi.org/10.1115/1.4040146.

24. Jouhara H, Chauhan A, Nannou T, Almahmoud S, Delpech B, Wrobel LC. Heat pipe based systems—advances and applications. Energy. 2017;128:729–54. https://doi.org/10.1016/j.energy.2017.04.028.

25. Khalid SU, Babar H, Ali HM, et al. Heat pipes: progress in thermal performance enhancement for microelectronics. J Therm Anal Calorim. 2020. https://doi.org/10.1007/s10973-020-09820-7.

26. Jyothi Sankar PR, Venkatachalapathy S, Asirvatham LG. Thermal performance enhancement studies using graphite nanofluid for heat transfer applications. Heat Transf. 2020. https://doi.org/10.1002/htj.21758.

27. Nazari MA, Ghasempour R, Ahmadi MH. A review on using nanofluids in heat pipes. J Therm Anal Calorim. 2019;137:1847–55. https://doi.org/10.1007/s10973-019-08094-y.

28. Jyothi Sankar PR, Venkatachalapathy S, Santhosh Kumar MC. Effect of hydrophilic coating on mesh wicks used in heat pipes. Surf Eng. 2019. https://doi.org/10.1080/02670844.2019.1695370.

29. Kumaresan G, Vijayakumar P, Ravikumar M, Kamatchi R, Selvakumar P. Experimental study on effect of wick structures on thermal performance enhancement of cylindrical heat pipes. J Therm Anal Calorim. 2019;136:389–400. https://doi.org/10.1007/s10973-018-7842-2.

30. Hopkins R, Faghri A, Khrustalev D. Flat miniature heat pipes with micro capillary grooves. J Heat Transf. 1999;121:102–9. https://doi.org/10.1115/1.2825922.

31. Liu ZH, Zhu QZ. Application of aqueous nanofluids in a horizontal mesh heat pipe. Energy Conv Manag. 2011;52:292–300.